HYDROGEN PERMEATION IN HSLA STEELS IN RELATION TO ITS STRESS CORROSION CRACKING BEHAVIOUR

F.Gutiérrez-Solana* and I.M.Bernstein**

This work analyzes, for two high strength low alloys steels, the relation between the influence of microstructural variation on SCC phenomena and associated changes in hydrogen permeation. Hydrogen permeation tests have been performed for differently heat treated samples. The results obtained for the solubility and diffusivity are correlated to the corresponding SCC behaviour in a 3.5% NaCl solution environment. From these correlations some understanding of how microstructure controls the SCC behaviour through its influence on the hydrogen diffusivity, has been demonstrated in mechanically stable and unstable microstructures.

INTRODUCTION

In previous works, (Bernstein and Thompson (1), Thompson and Bernstein (2), the important control that the microstructure has over the stress corrosion cracking (SCC) behaviour of high strength steels, especially when the corresponding mode of fracture is transgranular, has been analyzed.

In order to better understand this control, for the important case where SCC is a hydrogen assisted phenomenon (Ricker and Duquette (3)), this work analyzes the hydrogen permeation response of different microstructures of two steels. For all the microstructures, their corresponding SCC behaviour are then correlated to the permeation results to establish the important role of microstructural variations on SCC. The main variables are the diffusivity and the solubility of hydrogen as determined from electrochemical permeation tests.

* E.T.S. Ing. Caminos, Universidad de Cantabria, Santander, Spain.
** Metallurg Eng & Matl Science Dep Carnegie-Mellon University Pittsburgh U.S.A.

SCC BEHAVIOUR

Material Tested

HY130 and 300M steels were used in this work. Their corresponding chemical compositions are shown in table 1

TABLE 1 - Chemical Composition of the Steels used (weight %).

	C	Mn	Si	Cr	Ni	Mo	V
300M	0.39	0.80	1.68	0.76	1.74	0.40.	0.08
HY130	0.11	0.81	0.34	0.54	4.95	0.59	0.08

TABLE 2 - Description and mechanical Characterization of heat treated Samples.

Steel	Sample	Treatment	Yield Strength (MPa)
300M	M1	O.q. Temper 2 hrs at 450 °C	1400
	M2	O.q. Anneal 1 hr at 780 °C, o.q.	1600
	M3	O.q. Anneal 1 hr at 745 °C, o.q.	850
	M4	O.q. Anneal 1 hr at 780 °C, Isothermally transform 3 hrs at 350 °C	860
	M5	O.q. Temper 2 hrs at 650 °C	1030
HY130	HY0	Oil quenched	1090
	HY1	Isothermally transform 18 hrs at 395 °C	850
	HY2	Air cool	930
	HY3	O.q. Anneal 1 hr at 700 °C, O.q.	870
	HY4	O.q. Anneal 1 hr at 720 °C, O.q.	880
	HY5	O.q. Anneal 1 hr at 675 °C, O.q.	810
	HY6	O.q. Anneal 1 hr at 675 °C, Isothermally transform 3 hrs at 375 °C	750

O.q.= oil quenched
All the samples were austenitized 1 hour at 900 °C.

Heat Treatments

Different heat treatments were performed on the steels investigated in order to analyze the effect of the corresponding microstructural changes on the SCC behaviour. These treatments and their mechanical characterization defined by their yield strength, are described in table 2.

SCC Testing

SCC tests were performed for all cases on DCB type samples using a 3.5% NaCl + distilled water solution as an agressive environment. The testing method as well as the corresponding results have been previously reported (Kerr et al. (4)). Figure 1 summarizes the da/dt-K_I curves obtained, showing the important variation of SCC behaviour due to the microstructural changes associated with the different heat-treatments. To better appreciate the importance of this microstructural control, figure 2 represents the relation between the K_{ISCC} values and the corresponding yield strength, showing the improvements possible in both HY130 and 300M SCC behaviour without loss in strength, and even in some of the treatments (M5) associated with strength improvements. This SCC improvement is clearly associated with the corresponding changes in microstructure.

Microstructral Analysis

A complete microstructural analysis has been carried out by optical and electron (SEM and TEM) microscopy to understand the effect of each different type of microstructure on SCC. Table 3 summarizes the results of this analysis.
The correlation of this analysis with testing results showed that the untempered, dislocated or twinned martensite was the microstructure with the worst effect. Bainitic and, specially, dual-phase ferritic-martensitic microstructures enhance the resistance to the SCC phenomena. Finally, highly tempered martensite appears as the best microstructure to avoid SCC problems.

The presence of retained austenite, observed by TEM techniques, and could not be reproducably quantified but a closer determination of its quantity, and mechanical stability has been carried out by x-ray diffractometry (Miller (5)). The observed moderate improvement to SCC resistance was associated with the continuity and stability of this phase (300M steel). A less clearly defined influence of the role of mechanical transformation to martensite (HY130 steel), have been also analyzed (Gutiérrez-Solana et al. (6)).

Fractography

A complete SEM fractographical analysis has been done on the samples tested. In all the cases, HY130 samples showed a transgranular fracture mode, associated with the more important influence of microstructure on SCC response. For 300M steel, samples M1 and M2, with similar SCC behaviours, had an intergranular fracture mode; in all the other treatments the fracture path was transgranular, and associated again with a microstructural dependence on SCC behaviour.

TABLE 3 - Microstructral Characterization of Heat Treatments.

Steel	Sample	General Features	Retained %*	Austenite Distribution	Twinned Martensite
300M	M1	Dislocated, tempered martensite, principal carbide is cementite.	4/1	Discontinuous interlath film	Moderate
	M2	Lath and polygonal ferrite, dislocated martensite.	13-9	Semicontinuous interlath film	High
	M3	-	0	-	
	M4	Lath and polygonal ferrite, dislocated martensite, lower bainite	24/22	Continuous thick film	Low
	M5	Tempered martensite with intra- and interlath cementite.	0	-	-
HY130	HY0	Dislocated and autotempered martensite	0	-	High
	HY1	Broad lower bainite, dislocated martensite	3/2	Not imaged	High
	HY2	Dislocated martensite, presence of upper and lower bainite	7/4	Semicontinuous interlath film	Low
	HY3	Lath and polygonal ferrite, dislocated martensite	3/1	Discontinuous interlath film	Low
	HY4	-	0	-	-
	HY5	Lath and polygonal ferrite, dislocated martensite	11-4	Blocky, equiaxed with some films	Moderate
	HY6	Lath and polygonal ferrite, dislocated martensite	5/1	Blocky, equiaxed with some films	Low

* Unstrained retained austenite/10% strained.

HYDROGEN PERMEATION TESTS

The hydrogen permeation tests were performed using a double-cell electrolytic cell, figure 3, based on the electrochemical technique described in previous works (Devanathan and Stachurski (7), Pressouyre (8)).

The specimens used were mechanically and chemically thinned from 50 to 150 μm, in order to shorten the testing time, thereby minimizing complications due to solution concentration variations.

The specimens were also palladium plated to protect the steel from the reactions at the anodic side of the cell, and were tested at a cathodic current density of 1 mA/cm^2.

At least two transients were performed on each sample to correlate the results to the presence and the type of any existing hydrogen traps (Pressouyre (8), Iono and Yazima (9)).

Results

From the transients' flux-time curves, figure 4, the lattice diffusion constant, Do, can be deduced from the breakthrough time, t_b, and/or from the decay process, yielding the corresponding decay time constant. Also, the corresponding apparent diffusion constant, Dap, can be deduced from the corresponding time lag, t_{lag}. From this Dap value and the steady state flux, J_∞, the apparent solubility, Sap, can be determined using the relationship:

$$J_\infty = \frac{Dap \cdot Sap \cdot A}{L} \qquad (1)$$

where A = area of the cross-section of the specimen
L = thickness of the specimen.

Table 4 summarizes the values obtained for the diffusion constants, Do and Dapp, and solubility, Sapp, for each sample tested. As these results have to be compared to the SCC response of the corresponding treatment; the stage I threshold values, K_{ISCC}, and the stage II crack propagation rate, da/dt, have been also included at this table.

The amount of hydrogen trapping can be associated with the magnitude of the Do/Dap ratio, and the reversible or irreversible condition of the traps to the variation of this ratio from the first to the second permeation transient.

TABLE 4 - Results of Hydrogen Permeation and SCC Tests.

	300 M Samples				
	M1	M2	M3	M4	M5
SCC					
K_{ISCC} [MPa √m]	17	17	41	42	113
$(da/dt)_{II}$ [ms^{-1}]	5×10^{-7}	6×10^{-7}	7×10^{-8}	3×10^{-8}	1×10^{-9}
Diffusivity [cm^2/s]					
1st transient Do	5.8×10^{-8}	3.5×10^{-8}	1.0×10^{-7}	3.6×10^{-8}	1.9×10^{-7}
1st transient Dap	3.2×10^{-10}	3.4×10^{-11}	6×10^{-11}	1.4×10^{-10}	1.6×10^{-10}
2nd transient Dap	2.7×10^{-9}	9.7×10^{-10}	8.5×10^{-10}	8.1×10^{-10}	4.2×10^{-10}
Solubility [ppm]					
1st transient Sap	212	1984	1614	683	1052
2nd transient Sap	24	56	107	102	354

	HY 130 Samples					
	HY0	HY1	HY2	HY4	HY5	HY6
SCC						
K_{ISCC} [MPa √m]	31	41	53	67	99	142
$(da/dt)_{II}$ m s^{-1}]	3×10^{-8}	4×10^{-8}	3×10^{-8}	4×10^{-9}	2×10^{-9}	5×10^{-10}
Diffusivity [cm^2/s]						
1st transient Do	2.2×10^{-7}	1.7×10^{-7}	4.2×10^{-7}	1.1×10^{-7}	1.4×10^{-7}	4.7×10^{-8}
1st transient Dap	-	1.5×10^{-10}	6.3×10^{-10}	1.6×10^{-10}	3.2×10^{-11}	9.2×10^{-12}
2nd transient Dap	8.4×10^{-10}	1.1×10^{-9}	1.2×10^{-10}	2.5×10^{-10}	9.2×10^{-11}	8.4×10^{-12}
Solubility [ppm]						
1st transient Sap	-	360	490	2640	6640	4300
2nd transient Sap	450	260	430	1940	2970	44700

ANALYSIS OF THE SCC-PERMEATION RELATION

Crack Propagation

Considering SCC as an hydrogen assisted phenomenon, the crack propagation rate has been related to the diffusivity of hydrogen through the material (Thompson and Bernstein (2)).

To better appreciate the real control that the diffusivity exercises over the crack propagation rate, figure 5 shows the relation between both variables, da/dt and Dap, for the samples in this study.

It can be observed that when the fracture mode is intergranular, samples M1 and M2 of 300M steel, no correlation can be determined between mechanical and permeation variables, showing that this kind of crack propagation is not controlled by hydrogen diffusivity through the bulk material. Probably, other permeation paths, as grain boundaries, are more effective in controlling intergranular crack propagation.

For transgranular fracture processes, a relation can be observed, showing a slower propagation rate for microstructures with slower diffusivity. The 300M steel appears to be more susceptible to this effect than HY130. For the latter a more important drop of the crack propagation rate for a similar change in diffusion constant is observed leading to the lower slope seen in figure 5.

The more sensitive linear relation obtained for the 300M steel can be explained by the stability of the phases for all obtainable microstructures. Thus, for this steel when the fracture is transgranular, the rate of hydrogen diffusivity is the most important factor controlling the crack propagation rate.

On the contrary, HY130 does not show a linear behaviour (figure 5) because of the very low apparent diffusivity observed for samples HY5 and HY6. These contain significant amounts of retained austenite, which is not as effective in reducing the crack propagation rate as a linear extrapolation would suggest (dotted line). The mechanical instability of this austenite, which transforms to martensite at the crack tip plastic zone, acts as a source enhancer of hydrogen (Pressouyre (10)) since martensite has a much lower hydrogen solubility. So, for these samples, the presence of this unstable retained austenite and its corresponding transformation are controlling the magnitude of the crack propagation rate.

In both cases, a model based on a critical concentration of hydrogen, C_k, (Pressouyre (10), (11)) can explain the propagation process. Cracks propagate when the critical concentration of hydrogen is achieved at their tip, but this hydrogen has different ways to arrive at this zone: normal diffusion or release from the lattice following retained austenite transformation. Figure 6 is a sketch of how a model of this type can be correlate hydrogen permeation and crack propagation.

In a normal permeation process the hydrogen from irreversible traps is not released, and only that available from the lattice and reversible traps can aid the continuously moving crack tip. For this reason da/dt rates are better related to the second permeation transient diffusivity figure 5, which samples only reversible trap behaviour.

Initiation

Since the local hydrogen concentration depends on the diffusivity, (corrected by the effect of hydrogen released at unstable microstructures upon their transformations) and on the time and stress state (Doig and Jones (12)), the crack initiation process can be related to the critical value of this concentration, C_K, at infinite time ($t = \infty$), when the stress state corresponds to the K_{ISCC} stress intensity value.

From this, a relation between the critical concentration value and K_{ISCC} can be assumed, defined by the following expression.

$$\ln C_K = A(\sigma_y) + B\,K_{ISCC} \qquad (2)$$

Where A is a function of the yield strength and B is a constant that depends on material properties and environmental conditions.

The apparent solubility can be considered as an index of this critical concentration, particularly when the existing traps are not affected by hydrogen presence. Figure 7 shows the relation between ln Sap and the K_{ISCC} values.

For HY130 steel, as a general behaviour, K_{ISCC} increases with the apparent solubility, for both transients. Considering that expression (2) does not consider the hydrogen released from the retained austenite transformed at the plastic zone, only those samples without unstable retained austenite have been used to define the corresponding linear relationship and in particular the parametric function with yield strength.

The presence of unstable retained austenite produced a better resistance to SCC initiation than one would expect from considering only the solubility. This effect can be explained by considering the transformation process as an "energy trap", that creates the necessity of higher K_{ISCC} values to get to the critical conditions to initiate the rupture process (Gutiérrez-Solana et al. (6)).

For 300M steel, a clear difference is also seen in the solubility-initiation relation between samples with transgranular fracture mode and those with an intergranular one. The samples, M1 and M2, with intergranular fracture mode, do not show a relation between their K_{ISCC} values and their hydrogen solubility, indicating that in this case other variables have to control the SCC phenomena. For those showing a transgranular fracture mode, a linear relation is obtained between K_{ISCC} and solubility for values calculated from the second transient, indicating a possible control on the initiation of cracking from the hydrogen concentration at the reversible traps or the lattice.

CONCLUSIONS

In almost all the cases analyzed the corresponding microstructural dependence of the hydrogen permeation processes has been shown to control ensuing SCC processes.

For stable microstructures this correlation is considered to be a general rule, but when the microstructure contains mechanically unstable retained austenite, as in HY130 steels, the instability affects the SCC processes, either through its influence on hydrogen permeation by releasing additional hydrogen, aiding propagation, or by acting as an "energy trap", thereby delaying initiation.

SYMBOLS USED

da/dt = crack propagation rate (ms^{-1})

K_I = stress intensity factor (MPa $\sqrt{m}$)

K_{ISCC} = K_I at threshold in SCC process (MPa $\sqrt{m}$)

Do = lattice diffusion constant ($cm^2\ s^{-1}$)

Dap = apparent diffusion constant ($cm^2\ s^{-1}$)

Sap = apparent solubility (ppm)

σ_y = yield strength (MPa)

J = hydrogen flux

C_K = critical concentration of hydrogen at fracture conditions

REFERENCES

(1) Bernstein, I.M. and Thompson, A.W., Int. Metals Reviews, Vol. 21, 1976, pp. 187-269.

(2) Thompson, A.W. and Bernstein, I.M., Advances in Corrosion Science and Technology, Vol. 7, 1980, pp. 53-175.

(3) Ricker, R.E. and Duquette, D.J., "The Role of Environment on Time Depended Crack Growth". Technical Report NR 036-039, 1981.

(4) Kerr, R., Gutiérrez-Solana, F., Bernstein, I.M. and Thompson, A.W., "The Role of Microstructure on the Stress Corrosion Cracking of Medium to High Strength Steels", submitted to Metallurgical Transactions, 1985.

(5) Miller, R.L., Trans. of the ASME, Vol. 57, 1964, pp. 892-899.

(6) Gutiérrez-Solana, F., Takamadate, C., Thompson, A.W. and Bernstein, I.M., "Modeling the Effect of Retained Austenite on Stress Corrosion Cracking", submitted to Metallurgical Transactions, 1985.

(7) Devanathan, M.A.W. and Stachurski, Z., Proc. of the Roy. Society, Vol. 270-A, 1962, pp. 90-102.

(8) Pressouyre, G.M., Ph.D. Thesis, Carnegie-Mellon University, 1977.

(9) Iino, M. and Yazima, I., in "Hydrogen in Steel", University of Bath, 1982, pp. 14-16.

(10) Pressouyre, G.M., in "Current Solutions to Hydrogen Problems in the Steel", Proceedings, Washington, U.S.A., edited by Interrante, C.G. and Pressouyre, G.M., A.S.M., 1982, pp. 18-37.

(11) Pressouyre, G.M., in "Environmental Degradation of Engineering Materials", Lonthan, M.C. et al., Virginia Polytechnic University, 1981.

(12) Doig, P. and Jones, G.T., Metallurgical Transactions, Vol. 8A, 1977, pp. 1993-1998.

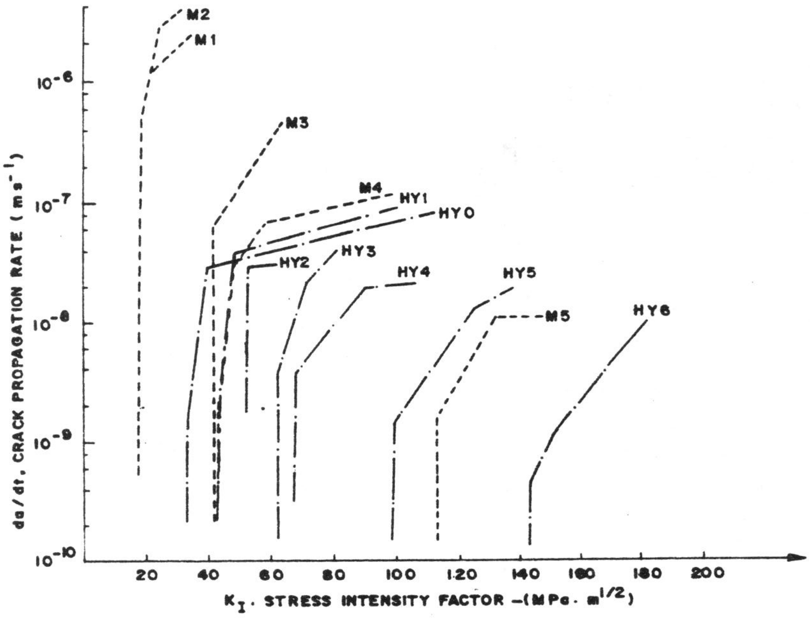

Figure 1 K_I-da/dt curves of SCC testing

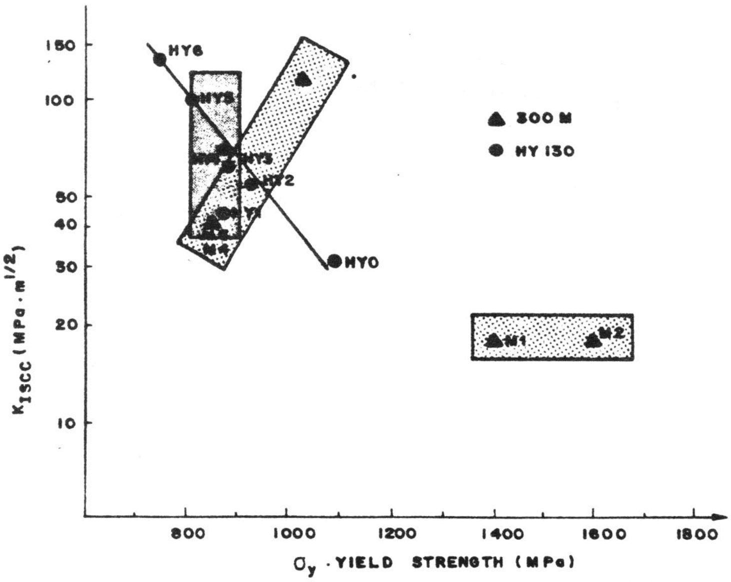

Figure 2 K_{ISCC} - σ_y relation

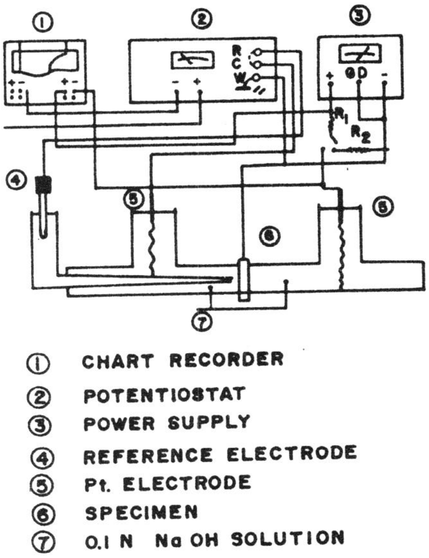

Figure 3.– Hydrogen permeation test system.

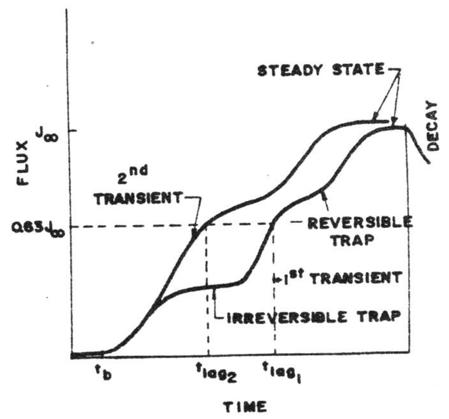

Figure 4.– Hydrogen flux-time curves.

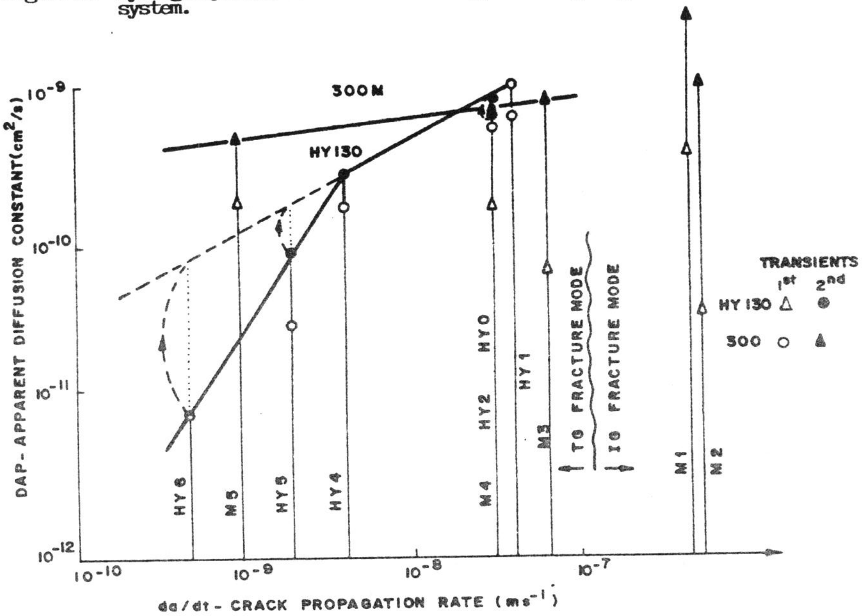

Figure 5.– da/dt – Dap relation.

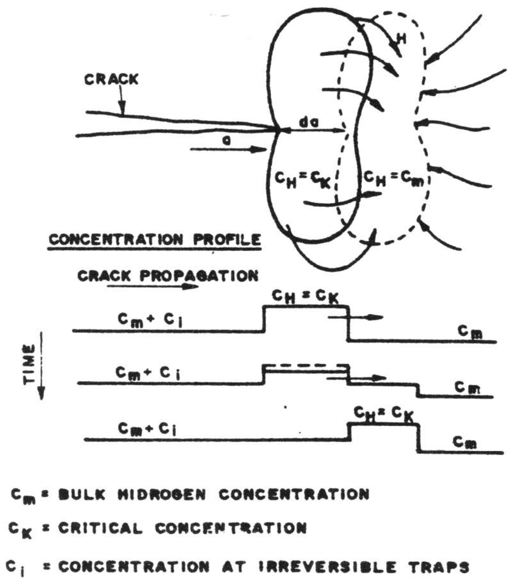

Figure 6.- Propagation model.

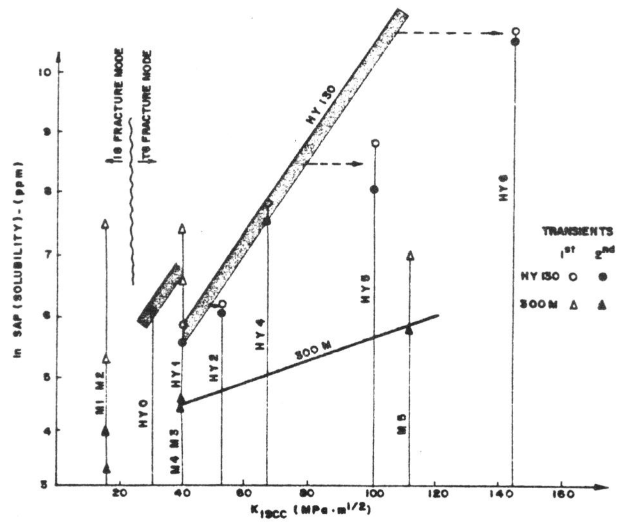

Figure 7.- K_{ISCC} – ln Sap relation.